Charged Higgs pair production in association with the Z^0 boson at electron-positron colliders

Nasuf Sonmez[*]

Department of Physics, Faculty of Science, Ege University, 35040 Izmir, Turkey

In this paper, the production of the charged Higgs pair associated with the Z^0 boson is analyzed in the minimal extension of the standard model, the so-called two-Higgs-doublet model. The process $e^+e^- \to H^+H^-Z^0$ is calculated at the tree level including all the possible diagrams in the two-Higgs-doublet model. The numerical analysis is performed in consideration of the current experimental constraints and various scenarios for the free parameters of the model. The results are presented as a function of the center-of-mass energy, the charged Higgs mass ($m_{H^\pm}$), and the ratio of the vacuum expectation values (t_β). The unpolarized cross section, taking into account the results in the flavor physics, gets up to 0.278 fb for $m_{H^\pm} = 175$ GeV, and it declines with decreasing $m_{H^\pm}$ in type I. However, it gets down to 0.073 fb for $m_{H^\pm} = 500$ GeV in type II. Further, the calculation is also carried out in the nonalignment scenario and low-m_{h^0} scenario. The effect of the polarized incoming e^+ and e^- beams shows that the cross section is enhanced by a factor up to 2.5 at P$(+0.60, -0.80)$ polarization configuration. Decay channels of the charged Higgs, possible final states of the process, and some differential distributions belonging to the charged Higgs and Z^0 boson are examined for each scenario. The analysis shows that some channels have a higher branching ratio such as $H^+ \to t\bar{b}$, $H^+ \to W^+h^0$, and $H^+ \to W^+H^0$. These decay channels are essential in the charged Higgs searches at the lepton colliders for the scenarios interested. The detection of the charged Higgs is a powerful sign for the extended scalar sectors, and the results show the potential of a future lepton collider.

I. INTRODUCTION

Over the last couple of decades, many extensions to cure the quadratic divergence at the scalar sector of the Standard Model (SM) has been proposed, and the implications of the new physics have been studied intensively. One possible extension of the SM is to add a second Higgs doublet to the scalar sector. These two Higgs doublets are defined to have the same quantum number so that they together could give mass to leptons, quarks, and electroweak bosons. The addition of an extra doublet to the scalar sector of the SM gives new couplings and interactions, consequently, a rich phenomenology is obtained in 2HDM. In general, there are two charged Higgs bosons ($H^\pm$) and three neutral Higgs bosons (h^0, A^0, H^0) [1,2] in 2DHM, and playing with the free parameters of the model h^0 could be set to resemble the discovered Higgs boson.

Nowadays, there is an ongoing effort for another project named the Linear Collider Collaboration (LCC); it is an organization that brings the two most likely candidates for the next collider program, the Compact Linear Collider Study (CLIC) and the International Linear Collider (ILC), together under one roof. When this project is constructed, e^+e^-, e^-e^-, and γe collisions will be studied. One of the primary tasks at the future lepton colliders is to complement the LHC results and also search for clues in beyond the SM such as supersymmetry, an extension of the scalar sector or exotic models. Both of the collider projects are designed to study the properties of the new particles and the interactions they might undergo according to the vast amount of theories. As it is known, the lepton colliders compared to the LHC have a cleaner background, and it is possible to extract the new physics signals from the background more easily.

There has been a long-time effort to observe a hint associated with a charged Higgs boson in the past and current experiments. However, it was not discovered at the LEP and Tevatron, and yet the search is still going on at the LHC [3]. The main discovery channel of the charged Higgs boson in the 2HDM is through the $e^+e^- \to H^+H^-$ or $e^+e^- \to H^\pm f f'$ channels. Such signals in the 2HDM are studied in Refs. [4,5]. On the other hand, the pair

[*]nasuf.sonmez@ege.edu.tr

production of the charged Higgs boson associated with a gauge boson is also possible at the lepton colliders where this process could be studied with more precision. The process $e^+e^- \rightarrow H^+H^-Z^0$ is complementary to the discovery of the charged Higgs pair production. The process would also give a way to measure the couplings $c_{H^+H^-h^0}$ and $c_{H^+H^-H^0}$. These couplings along with the other trilinear Higgs couplings will help us to reconstruct the Higgs potential.[1] The process was investigated before in Ref. [6] for a case study in which the triple Higgs couplings were studied, and the diagrams that are sensitive to the triple Higgs couplings were included in the calculation. The same process was investigated in the left-right twin Higgs model in which doubly charged Higgs pair production with Z^0 boson was analyzed [7], and a similar process in the Higgs triplet model was examined in Ref. [8]. In this work, the production of the $H^+H^-Z^0$ including all the possible diagrams at the Born level is calculated. Numerical analysis of the total cross section is performed as a function of the c.m. energy, the charged Higgs mass, and the free parameters of the 2HDM for the benchmark scenarios with various motivations. In addition to these, the results with different beam polarizations are presented. A discussion is carried on the couplings essential in the production of $H^+H^-Z^0$ and decay channels of the charged Higgs boson for each scenario. A preliminary calculation of the differential cross section as a function of the kinematical properties of the Z and the $H^\pm$ boson is obtained. Each scenario with subsequent decay channels of $H^\pm$ is explored for later Monte Carlo studies.

The content of this paper is organized as follows. In Sec. II, the scalar sector, free parameters of the model, and

the masses of the Higgs bosons in 2HDM are reviewed. The machinery, the work flow of the analysis, and the kinematics of the scattering process are explained in Sec. III. The constraints coming from the experimental results are underlined in Sec IV. Numerical analysis is performed on three scenarios, which are named as the nonalignment scenario, low-m_H mass scenario, and favored region in light of the flavor physics results. The numerical results for each of the scenarios, including the beam polarization, are presented thoroughly in Sec V. Decay channels of the charged Higgs and identification of the process are discussed along with the differential distributions in Sec VI. The conclusion is drawn in Sec VII.

II. SCALAR SECTOR AND THEORETICAL FRAMEWORK FOR 2HDM

In this section, the phenomenology of the 2HDM, the scalar sector, and the free parameters in the model are presented. The model itself and the detailed introduction of the framework have been studied before by many authors, and they are given in Refs. [2,9–11]. Therefore, only a short review of the 2HDM that is relevant to the analysis is presented. The 2HDM is constructed by adding a second $SU(2)_L$ Higgs doublet with the same hypercharge ($Y = 1$) to the scalar sector. If we denote the Higgs doublets as

$$\Phi_i = \begin{pmatrix} \phi_i^+ \\ \frac{1}{\sqrt{2}}[v_i + \rho_i + i\eta_i] \end{pmatrix}, \tag{1}$$

with the scalar potential of the 2HDM given in Eq. (2), there will be in total 14 free parameters:

$$V(\Phi_1, \Phi_2) = m_{11}^2|\Phi_1|^2 + m_{22}^2|\Phi_2|^2 - [m_{12}^2\Phi_1^\dagger\Phi_2 + \text{H.c.}] + \frac{\lambda_1}{2}|(\Phi_1^\dagger\Phi_1)^2 + \frac{\lambda_2}{2}(\Phi_2^\dagger\Phi_2)^2 + \lambda_3|\Phi_1|^2|\Phi_2|^2 + \lambda_4|\Phi_1^\dagger\Phi_2|^2$$

$$+ \left[\frac{\lambda_5}{2}(\Phi_1^\dagger\Phi_2)^2 + (\lambda_6(\Phi_1^\dagger\Phi_1) + \lambda_7(\Phi_2^\dagger\Phi_2))\Phi_1^\dagger\Phi_2 + \text{H.c.}\right]. \tag{2}$$

In general, the parameters m_{11}, m_{22}, and $\lambda_{1,2,3,4}$ are real, while m_{12} and $\lambda_{5,6,7}$ are complex. Both of the doublets have the same charge assignment, and they could couple to leptons and quarks as in the SM. However, to suppress the CP violation and the flavor-changing neutral currents (FCNCs) at the tree level, the construction of the model needs to be constrained in some way. Traditionally, a discrete symmetry ($\mathcal{Z}_2$) was introduced, which puts restrictions on the most general form of the Higgs scalar potential and the Higgs-fermion interactions [12–14]. Discrete $\mathcal{Z}_2$ symmetry is simply defined as the invariance of the

Lagrangian under the interchange of $\Phi_1 \rightarrow \Phi_1$ and $\Phi_2 \rightarrow -\Phi_2$ (in a generic basis). If the discrete $\mathcal{Z}_2$ symmetry is extended to the Yukawa sector, then the interactions between Higgses and fermions could be written in four different and independent ways. These are called type I through type IV, and they will be explained later. Since we do not care about the CP violation, we set $\lambda_6 = \lambda_7 = 0$. Then, the complex parameters m_{12} and λ_5 are taken as real. As a result, the free parameter number reduces to 8 under these assumptions. If this symmetry is allowed to violate softly, then FCNCs are naturally suppressed at the tree level. The m_{12}^2 term in Eq. (2) ensures the breaking of the discrete symmetry softly.

The mass spectrum of the Higgs bosons is computed first by imposing the constraints obtained from the potential minimum condition ($\partial V/\partial\Phi_i = 0$, for $i = 1$, 2) and

---

[1]It should be noted that the complete reconstruction of the Higgs potential requires the measurement of the quartic Higgs couplings as well.

eliminating m_{11} and m_{22}. Second, the Higgs doublets are defined as given in detail in Refs. [1,9,15,16]. After decomposing the scalar potential into a quadratic term plus cubic and quartic interactions, the mass terms are extracted. Finally, diagonalizing the quadratic terms, we easily obtain the physical Higgs states and their masses. The masses of the charged and the CP-odd Higgs states are defined as

$$m_{A^0}^2 = \frac{m_{12}^2}{\sin\beta\cos\beta} - 2\lambda_5 v^2 \tag{3}$$

$$m_{H^\pm}^2 = m_{A^0}^2 + (\lambda_5 - \lambda_4)v^2, \tag{4}$$

where β is the ratio of the vacuum expectation value of the Higgs doublets ($\tan\beta = v_1/v_2$). The mass of the CP-even states becomes

$$\begin{pmatrix} h^0 \\ H^0 \end{pmatrix} = \mathcal{R} \begin{pmatrix} m_{12}^2\tan\beta + \lambda_1 v_1^2 & -m_{12}^2 + \lambda_{345}v_1 v_2 \\ -m_{12}^2 + \lambda_{345}v_1 v_2 & m_{12}^2\cot\beta + \lambda_2 v_2^2 \end{pmatrix} \mathcal{R}^T, \tag{5}$$

where $\mathcal{R}$ is a unitary rotation matrix that diagonalizes the CP-neutral Higgs mass matrix [1,10] as a function of the angle $(\beta - \alpha)$, $\lambda_{345} = \lambda_3 + \lambda_4 + \lambda_5$, and $v_1 = v\sin\beta$, $v_2 = v\cos\beta$ so $v = \sqrt{v_1^2 + v_2^2} = 246$ GeV. Then, the physical neutral CP-even scalar states are obtained by orthogonal combinations of ρ_1 and ρ_2 given in Eq. (1). A lighter h^0 and a heavier H^0 boson are defined as $h^0 = \rho_1\sin\alpha - \rho_2\cos\alpha$ and $H^0 = \rho_1\cos\alpha - \rho_2\sin\alpha$. Accordingly, the SM Higgs boson would be

$$H^{SM} = \rho_1\cos\beta + \rho_2\sin\beta \tag{6}$$

$$= h^0 s_{\beta\alpha} + H^0 c_{\beta\alpha}, \tag{7}$$

where the angle that rotates the CP-even Higgs states is defined as $s_{\beta\alpha} = \sin(\beta - \alpha)$, $c_{\beta\alpha} = \cos(\beta - \alpha)$. If $s_{\beta\alpha} = 1$, which is called the *SM-alignment limit* [17–20], is assumed, an important feature shows up: the ratio of the couplings between h^0 (H^0) and the SM gauge bosons ($V = W^\pm/Z^0$) to the corresponding SM Higgs one will be $c_{VVh^0}/c_{VVH_{SM}} = s_{\beta\alpha}$ ($c_{VVH^0}/c_{VVH_{SM}} = c_{\beta\alpha}$). Therefore, the lighter CP-even Higgs boson (h^0) becomes indistinguishable from the Standard Model Higgs boson, and H^0 acts as gaugephobic ($c_{\beta\alpha} = 0$) in this limit. In the literature, to explore the phenomenology of heavier CP-even boson (H^0), it is custom not to set $s_{\beta\alpha}$ to unity. That is also explored, and small deviations from unity are considered in the numerical calculation. The rest of the degree of freedom makes the prominent property of the model: two charged Higgs bosons and three neutral Higgs bosons [2]. In conclusion, the free parameters of the model are the masses of the neutral Higgs bosons ($m_{h/H^0/A^0}$) and the charged Higgs bosons ($m_{H^\pm}$), the ratio of the vacuum expectation values ($t_\beta = v_2/v_1$), the mixing angle between the CP-even neutral Higgs states (α), and the soft breaking scale of the discrete symmetry m_{12} [17].

III. CALCULATING THE CROSS SECTION

In this section, the analytical expressions, the vertices, and the Feynman diagrams relevant to the scattering process $e^+e^- \to H^+H^-Z^0$ are presented. Throughout this paper, the process is denoted as
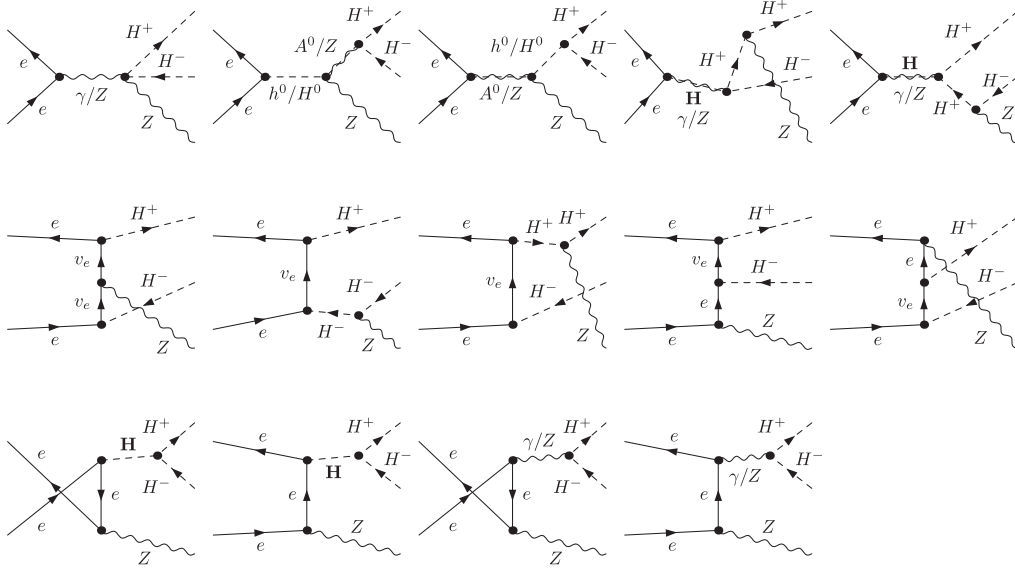

FIG. 1. All the Feynman diagrams that contribute to the scattering process $e^+e^- \to H^+H^-Z^0$ at the tree level. The dashed-wavelike line represents the nature of the propagating particle; vector boson (γ/Z-boson) or scalar particle ($h^0/H^0/A^0$). The bold **H** represents any of the $h^0/H^0/A^0$ bosons.

$$e^+(\mu) + e^-(\nu) \to H^+(k_3) + H^-(k_4) + Z^0(k_5),$$

where k_a ($a = 3, 4, 5$) are the 4-momenta of the outgoing charged Higgs boson pair and Z^0 boson. Additionally, the positrons and the electrons are characterized by their spin polarization μ and ν. Feynman diagrams that contribute to the process $e^+e^- \to H^+H^-Z^0$ at the tree level are shown in Fig. 1, which is produced with the help of FEYNARTS. The 2HDM Lagrangian and the corresponding vertices are calculated easily using FEYNRULES [21,22]. If there is a scalar particle in the model, there is a possibility of a scalar mediator between the incoming and outgoing states as seen in Fig. 1. Then, these s-channel diagrams make a significant contribution, but they are almost negligible away from the mass pole of the mediator. In any case, the narrow-width approximation for the scalars are employed, and the decay widths of the additional Higgs states are calculated with the help of 2HDMC [23] for each scenario. The analysis reveals that the couplings $c_{H^+H^-h^0}$ and $c_{H^+H^-H^0}$ make the dominant contribution to the cross section. All the vertices involved in the scattering process are given in Table I.

Another way to suppress the FCNCs in the Yukawa sector is to impose a natural condition that is to take the two Yukawa matrices to be aligned (Eq. (2.7) in Ref. [24]), and the Z_2 symmetric types are assumed as the particular cases of this aligned model. There, the ζ_L is the factor that defines the Yukawa coupling structure, namely, types I through IV. As follows, $\zeta_L = 1/t_\beta$ in type I and type IV, and it is defined as $\zeta_L = -t_\beta$ in types II [24] and III. For that reason, the numerical results presented in this work hold for types III and IV as well. With all the couplings defined,

TABLE I.   The quartic and the trilinear couplings involved in the scattering process. The weak angle and the other mixing angles are abbreviated as $s_w = \sin\theta_w$, $c_w = \cos\theta_w$. $s_{\alpha\beta} = \sin(\alpha + \beta)$, and $c_{\alpha\beta} = \cos(\alpha + \beta)$.

$c_{H^+H^-\gamma Z^0}$	$\frac{ie^2}{c_w s_w}(c_w^2 - s_w^2)$
$c_{H^+H^-Z^0Z^0}$	$\frac{ie^2}{2c_w^2 s_w^2}(c_w^2 - s_w^2)^2$
$c_{Z^0Z^0[h^0,H^0]}$	$\frac{iem_w}{2c_w^2 s_w}[s_{\beta\alpha}, c_{\beta\alpha}]$
$c_{H^+H^-\gamma}$	ie
$c_{H^+H^-Z^0}$	$\frac{ie}{2c_w s_w}(c_w^2 - s_w^2)$
$c_{H^+H^-h^0}$	$\frac{i}{v}((m_{h^0}^2 - 2m_{H^\pm}^2)s_{\beta\alpha} - (2m_{h^0}^2 - \frac{2m_{12}^2}{s_\beta c_\beta})\frac{c_{\alpha\beta}}{s_{2\beta}})$
$c_{H^+H^-H^0}$	$\frac{i}{v}((m_{H^0}^2 - 2m_{H^\pm}^2)c_{\beta\alpha} - (2m_{H^0}^2 - \frac{2m_{12}^2}{s_\beta c_\beta})\frac{s_{\alpha\beta}}{s_{2\beta}})$
$c_{e\bar{e}[h^0,H^0]}$	$-\frac{im_e}{v}[(s_{\beta\alpha} + c_{\beta\alpha}\zeta_L), (-c_{\beta\alpha} + s_{\beta\alpha}\zeta_L)]$
$c_{\nu_e\bar{e}H^+}$	$\frac{i\sqrt{2}m_e}{v}\zeta_L$

TABLE II.   Polarization configuration of the incoming beams used in this study are denoted by left ($-$) and right ($+$).

Pol-1	P_{e^+}, P_{e^-}	$(+0.3, -0.8)$
Pol-2	P_{e^+}, P_{e^-}	$(+0.6, -0.8)$

the amplitude for each of the diagrams are constructed using FEYNARTS [25,26]. Next, the simplification of the fermion chains, squaring the corresponding amplitudes, and the numerical analysis is accomplished using FORMCALC [27] routines.

After squaring the amplitude, a summation over the polarization vectors of the final states and averaging over the helicities of the initial states are performed. Finally, the total unpolarized cross section is defined as an integral over a four-fold differential cross section [28],

$$\sigma = \frac{1}{4}\sum_{\mu,\nu}\int_{m_{Z^0}}^{(k_5^0)_{\max}} dk_5^0 \int_{(k_3^0)_{\min}}^{(k_3^0)_{\max}} dk_3^0 \int_{-1}^{+1} d\cos\theta$$

$$\times \int_0^{2\pi} d\eta \frac{d^4\sigma_{\mu\nu}}{dk_5^0 dk_3^0 d\cos\theta d\eta}, \tag{8}$$

where the energy of the k_3 and k_5 is defined below and $a = \sqrt{s} - k_5^0$,

$$(k_3^0)_{\min,\max} = \frac{1}{2}\left[a \pm |\vec{k}_5|\sqrt{1 - \frac{4m_{H^\pm}^2}{a^2 - |\vec{k}_5|^2}}\right] \tag{9}$$

$$(k_5^0)_{\max} = \frac{s - 2m_{H^\pm}^2 + m_{Z^0}^2}{2\sqrt{s}}. \tag{10}$$

One other option at the linear collider (LC) is to polarize the incoming beams, which could maximize the physics potential, both in the performance of precision tests and in revealing the properties of the new physics beyond the SM. In this study, we also explored the dependence of the cross section on the polarization of the incoming electron and positron beams. The polarization of the incoming beam is significant especially to enhance some of the helicity channels. In annihilation diagrams, typically in the s channel, the helicities of the incoming beams are coupled to each other. For that reason, the helicities of the incoming particles in the SM need to be opposite of one another to recombine into the vector boson mediator, the Z^0 boson, or the photon. In exchange diagrams, the helicities of the incoming beams are directly coupled to the helicities of the final states. In this case, all helicity configurations for the beams are in principle possible.

The expression for the cross section for an arbitrary degree of longitudinal beam polarization is defined as

$$\sigma(P_{e^+}, P_{e^-}) = \frac{1}{4}[+(1 - P_{e^-})(1 + P_{e^+})\sigma_{LR}$$

$$+ (1 + P_{e^-})(1 - P_{e^+})\sigma_{RL}], \tag{11}$$

where σ_{LR} denotes the cross section for the 100% left-handed positron and 100% right-handed electron polarization. They are given in Table 2. P_{e^-} and P_{e^+} denote the

percentages of the electron and positron beam polarization, respectively. The σ_{LL} and σ_{RR} configurations are omitted due to the negligible contributions in Eq. (11). In this study, we examined various polarization configurations in a linear collider, which we present in the next sections. Two of these configurations are inspired by the ILC, which in pol-1 (pol-2) is defined as a right-handed positron with 30% (60%) polarization [29,30] and an electron with 80% left-handed polarization in both cases.

IV. CONSTRAINTS FROM THEORY AND EXPERIMENTS, BENCHMARK POINTS

There are two sets of constraints in the 2HDM: one is the theoretical constraints that come from the theory itself, and the other one is the results coming from the measurements carried out in the past and current experiments. These constraints need to be applied to the free parameters defined in the previous section.

A. Theoretical constraints

Perturbative unitarity is a requirement that comes from the fact that the scattering amplitudes need to be flat at the asymptotically high energies. Because of the additional Higgs states in the 2HDM, we need to make sure that Higgs-Higgs and Higgs-vector boson scattering cross sections are bounded by 16π [31].

Perturbativity is a theory that needs to be inside the perturbative region. The perturbative region is defined as the region in which all the quartic couplings in the theory are small, and we take them to be $|\lambda_i| \leq 4\pi$.

Vacuum stability is the scalar potential defined in Eq. (2) and needs to be positive in any direction of the field space, even at the asymptotically large values [32–36]. The stability constraint is translated into the following conditions:

$$\lambda_1 > 0, \qquad \lambda_2 > 0,$$
$$\lambda_3 + \sqrt{\lambda_1 \lambda_2} > 0,$$
$$\sqrt{\lambda_1 \lambda_2} + \lambda_3 + \min(0, \lambda_4 - |\lambda_5|) > 0.$$

B. Experimental constraints

The ATLAS and CMS experiments at the LHC have reported the so-long-hunted resonance with a mass of 125.4 ± 0.4 GeV [37–42]. That resonance needs to be of a CP-even nature, and for that reason, the particle at 125.4 GeV needs to correspond to one of the CP-even h^0 or H^0 states in 2HDM. In the numerical calculation, we considered both of these possibilities and investigated the implications on the cross section of $e^+ e^- \to H^+ H^- Z^0$. If we assume that h^0 is the discovered particle at the LHC, that puts a restraint on the couplings. Therefore, $s_{\beta-\alpha}$ is pushed to unity. In the opposite case, if the H^0 boson is assumed to be the discovered one, then $c_{\beta\alpha}$ needs to be set

to unity. However, we let that factor deviate from unity just for the sake of phenomenological curiosity.

The 2HDM needs to be compatible with the full set of electroweak precision observables, which are measured in the previous experiments [43]. There are parameters S, T, and U, which are called oblique parameters [44,45], and they merely represent the radiative corrections to the two-point correlation functions of the electroweak gauge bosons. These parameters are sensitive to any new physics contribution, and they take the value of the top-quark and Higgs masses so that they are set to vanish for a reference point in the SM ($S = T = U = 0$). According to that, a sizable deviation from zero would be an indicator of the existence of new physics. These oblique parameters have been calculated by Refs. [46–49] for the scenarios presented in the next section with the help of 2HDMC, and in all cases, the oblique parameters are much less than 10^{-2}.

The LEP experiment excluded the charged Higgs boson with a mass below 80 GeV (type-II scenario) or 72.5 GeV [50] (type-I scenario, for pseudoscalar masses above 12 GeV) at the 95% C.L. If it is assumed that $\mathcal{B}(H^+ \to \tau^+ \nu) = 1$, then the charged Higgs mass bound increases to 94 GeV for all $\tan\beta$ values. [51]. The Tevatron experiments D0 [52–54] and CDF [55] excluded the charged Higgs mass in the range of 80 GeV $< m_{H^\pm} <$ 155 GeV at the 95% C.L. assuming $\mathcal{B}(H^+ \to c\bar{s})$. The search on charged Higgs is also carried out at the LHC in the decay of top quark [56,57], and upper limits are set on the $\mathcal{B}(t \to H^+ b)$ and $\mathcal{B}(H^+ \to \tau\nu)$. More recent results are given in Ref. [58] and the references therein.

It is known that charged scalar states in the 2HDM affect the flavor physics, particularly $B_s \to X_s\gamma$ or $B_s \to \mu\mu$. In general, the flavor observables in these models are sensitive to the $m_{H^\pm}$ and $\tan\beta$. According to Refs. [59,60], $\bar{B} - B$ mixing disfavors $\tan\beta < 0.5$ and also lets the couplings of the Higgs to heavy quarks be in the perturbative region $t_\beta < 60$ [61,62]. More discussion is carried out in Ref. [50] and the references therein.

C. Benchmark points

Recognizing all these experimental and theoretical constraints, the following scenarios and benchmark points are chosen. These points are preferred by aiming at a broader survey of the region of phenomenological interest. As it is stated in the experimental constraints, we employed the 2HDMC [23] to check whether the theoretical constraints for each benchmark point are fulfilled:

(i) *Nonalignment scenario.*—This benchmark point is taken from Ref. [63], in which the particle with the mass of 125 GeV is interpreted as the lightest CP-even Higgs boson (h^0) with SM-like couplings. In the so-called alignment limit where $|c_{\beta\alpha}| \to 0$, the c_{hVV} coupling approaches the corresponding SM value, in which case the heavier CP-even

TABLE III. Benchmark points for the nonalignment scenario; all masses are given in GeV.

Benchmark	Yukawa Types	m_{h^0}	m_{H^0}	$c_{\beta\alpha}$	Z_4	Z_5	Z_7	t_β
1	Type I	125	(150…600)	0.1	−2	−2	0	(1…50)
2	Type II	125	(150…600)	$0.01(\frac{150 \text{ GeV}}{m_{H^0}})^2$	−2	−2	0	(1…50)

TABLE IV. Benchmark points for the low-m_H mass scenario; all masses are given in GeV.

Benchmark	Yukawa Types	m_{h^0}	m_{H^0}	$c_{\beta\alpha}$	Z_4	Z_5	Z_7	t_β
1	Type I	(65…120)	125	1.0	−5	−5	0	1.50
2	Type II	(65…120)	125	1.0	−5	−5	0	1.50

Higgs boson H^0 could not decay into W^+W^-/ZZ. The alignment limit is also endorsed by the additional Higgs boson searches at the LHC. However, to allow some interesting phenomenology for the heavier CP-even state (H^0), this benchmark is defined with a nonalignment ($c_{\beta\alpha} \neq 0$) as allowed by the present constraints. With this motivation, the masses of the other Higgs states A^0 and $H^\pm$ are taken as degenerate, and they are allowed to decouple $m_{h^0} = 125 < m_{H^0} < m_{A^0} = m_{H^\pm}$. Detailed analysis is carried out in Ref. [63], and the charged Higgs mass is given in the hybrid base as

$$m_{H^\pm}^2 = m_{A^0}^2 = m_{H^0}^2 s_{\beta\alpha}^2 + m_{h^0}^2 c_{\beta\alpha}^2 - Z_5 v^2, \quad (12)$$

where Z_5 is the quartic coupling parameter, and it is set to −2 along with Z_4. In this scenario, t_β and m_{H^0} are taken as a free parameters, and their ranges, as well as the other parameters, are given in Table III.

(ii) *Low-m_H mass scenario.*—As it is known, there are two CP-even states (h^0/H^0) in the 2HDM. In the previous scenario, it is assumed that the discovered scalar particle at the LHC in 2012 is the lighter CP-even Higgs (h^0) state. However, there is one other possibility that it could be the heavier CP-even Higgs (H^0) state. In that case, the coupling of the heavier CP-even Higgs to gauge bosons (c_{HVV}) will be scaled by a factor of $c_{\beta\alpha}$ instead of $s_{\beta\alpha}$, and as in the previous case, that also forces us to $c_{\beta\alpha} \approx \pm 1$. Because of the direct search limits, couplings of h^0 to vector bosons need to be suppressed heavily and even close to zero ($s_{\beta\alpha} \to 0$). This scenario is analyzed in detail in Ref. [63], in which the region $90 < m_h < 120$ GeV is not rejected by the LHC constraints (from $h^0 \to bb, \tau\tau$), which puts an upper limit on t_β. According to the authors, it is also possible to set exact alignment ($c_{\beta\alpha} = 1$) with either type-I or type-II Yukawa couplings. Therefore, choosing a nonaligned value for $c_{\beta\alpha}$ does not make

much of an impact on the production of the cross section, but more on that is delivered in the results. In Table IV, the free parameters are depicted in the hybrid base in which $Z_4 = Z_5$ is taken so that in particular the T oblique parameter cannot receive sizable contributions (Eq. (76) in Ref. [63]).

(iii) *Favored region in light of the recent experimental constraints.*—Taking into account all the recent updates particularly coming from the flavor physics, as the last scenario, we explored the region inspired by the results presented in Ref. [24]. Since the charged Higgs boson can contribute to flavor observables via the charged currents, flavor observables are quite significant. Motivated by the Ref. [24], the same masses for all the Higgs bosons were set $m_{H^0} = m_{A^0} = m_{H^\pm}$, and that also satisfied the theoretical constraints. The $s_{\beta\alpha}$ was set approaching the unity, which guaranteed that all the light Higgs self-couplings were close to the SM ones. In that case, the heavier CP-even Higgs boson (H^0) cannot decay into W^+W^- and ZZ pairs. According to the authors [24], in type I, $t_\beta < 1$ was strongly constrained by $\mathcal{B}(B_s^0 \to \mu^+\mu^-)$ and the mass difference of the scalars. However, the mass of the scalars was not constrained on the large t_β range compared to type II. The cross section in type II, as in type I, was calculated by setting the same masses for all the extra scalars. $s_{\beta\alpha}$ was taken to unity, and due to the dominant constraints from $\mathcal{B}(B \to \tau\nu)$ and $\mathcal{B}(B_q^0 \to \mu^+\mu^-)$, high t_β were excluded. The parameter region is defined in Table V, and more detailed

TABLE V. Benchmark points for the favored region in light of the recent experimental constraints in flavor physics; all masses are given in GeV.

Benchmark	Yukawa Types	m_{h^0}	$m_{(H^0/A^0/H^\pm)}$	$s_{\beta\alpha}$	t_β
1	Type I	125	(150…1000)	1.0	(1…50)
2	Type II	125	(500…1000)	1.0	(1…40)

discussion is given in Ref. [24] (particularly Fig. 3 and the references therein). In this basis, one other parameter required for the calculation was the m_{12}^2. The region for the m_{12}^2, where the theoretical constraints were fulfilled, was calculated with the help of 2HDMC.

V. NUMERICAL RESULTS AND DISCUSSION

In this section, the numerical results for the charged Higgs pair production associated with the Z^0 boson in an e^+e^- collider are presented and discussed for each scenario. The current parameters of the SM are taken from Ref. [64], in which $m_e = 0.51099892$ MeV, $m_Z = 91.1876$ GeV, $s_w = 0.222897$, and $\alpha = 1/137.035999$ are set. Taking into account all these constraints, the numerical analysis is carried out for unpolarized and polarized incoming beams.

A. Nonalignment scenario

The cross section of the process $(e^+e^- \rightarrow H^+H^-Z^0)$ was computed for the parameters presented in the nonalignment scenario [63]. In Fig. 2, we plotted the cross section as a function of the c.m. energy in the $1 < \sqrt{s} < 3$ TeV range and for two distinct charged Higgs masses $(m_{H^\pm})$. We also explored the polarization configurations of the incoming beams. As seen in Fig. 2, the cross section σ_{RL}, which represents the totally right-handed polarized e^+ beam and totally left-handed polarized e^- beam, is always greater than other polarization cases. In Fig. 2 (left), the cross section for polarized incoming beams has a value of $\sigma_{RL} \approx 0.368$ fb around $\sqrt{s} = 2.2$ TeV, whereas in the opposite helicity configuration, the cross section is $\sigma_{LR} \approx 0.057$ fb. The neutral Higgs mass was set to $m_{H^0} = 200$ GeV, and

the Yukawa couplings were in the type-I configuration. The total unpolarized cross section (σ_{UU}) was calculated, and it was around 0.106 fb. Since the polarization of the colliding beams let us study and tune various couplings of the model, we also produced the distribution of the cross section for two possible polarization cases in the LC. The cross section had a value of $\sigma_{\text{pol-1}} \approx 0.217$ fb, and in the other polarization configuration in which the positron was polarized right-handed by 60%, the cross section got up to $\sigma_{\text{pol-2}} \approx 0.266$ fb for type I in Fig. 2 (left). A large separation between $m_{H^\pm}$ and m_{A^0} was strongly constrained by the vacuum stability and perturbativity; for that reason, the calculation was carried in the limit of $m_{A^0} \sim m_{H^\pm}$ in the nonalignment scenario. Therefore, any value of m_{A^0} was allowed by the electroweak (EW) precision tests.

In Fig. 2 (right), the production rate of $H^+H^-Z^0$ was plotted for various polarization configurations, and type II was set. The unpolarized cross section was $\sigma_{UU} = 0.068$ fb at $\sqrt{s} = 2.9$ TeV. However, the polarized cross sections were $\sigma_{\text{pol-1}} \approx 0.137$ fb and $\sigma_{\text{pol-2}} \approx 0.167$ fb.

Two-dimensional analysis of the cross section of the process is drawn in Fig. 3 as a function of the c.m. energy and the charged Higgs mass $(m_{H^\pm})$. In Fig. 3, left, the nonalignment scenario with type-I Yukawa couplings is set, and on the right, the same analysis with type II couplings is displayed. The charged Higgs mass is computed by Eq. (12), and we scanned in the allowed range $379 < m_{H^\pm} < 690$ GeV for this scenario. According to the couplings given in Table I, the $m_{H^\pm}$ dependence appeared only in the CP-even to charged Higgs pair couplings. Indeed, in the nonalignment scenario, $c_{H^+H^-h^0}$ was the dominant coupling affecting the cross section. Choosing type I over type II affected only the $c_{e^+\nu_e H^+}$ and the $c_{e\bar{e}[h^0,H^0]}$ couplings.
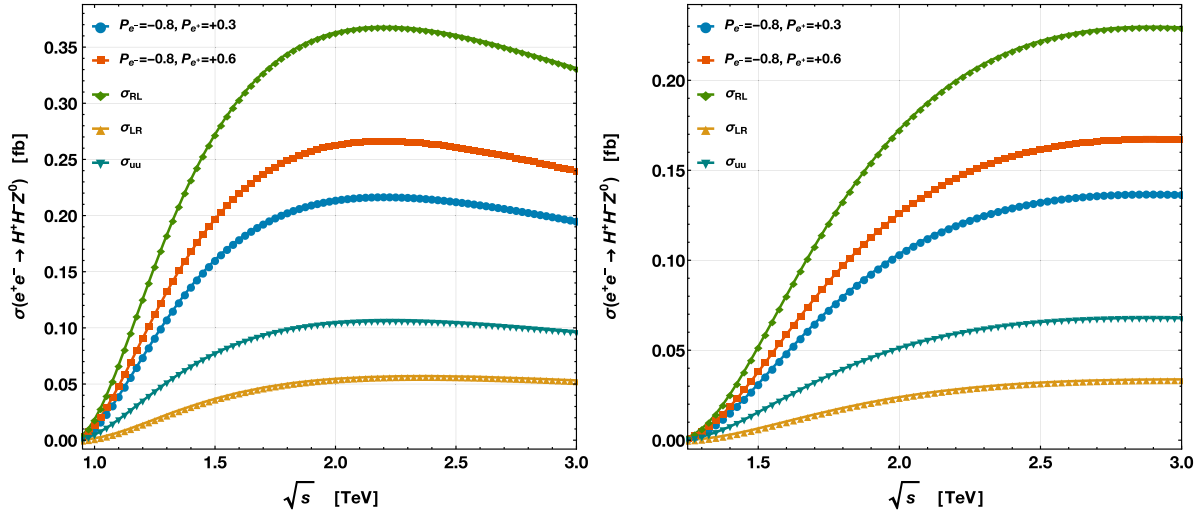

FIG. 2.   Comparison among various polarization cases for two benchmark points in the nonalignment scenario. The polarization configurations are depicted in the figure. (left): $c_{\beta\alpha} = 0.1$, $t_\beta = 45$, $m_{H^0} = 200$ GeV, and type I is set. σ_{LR}, σ_{RL}, and σ_{UU} represent the possible helicity configuration of the incoming positron and electron beams. (right): The same caption as the left figure, but $c_{\beta\alpha} = 0.01(\frac{150}{m_{H^0}})^2$, $m_{H^0} = 425$ GeV, and type II is assumed.
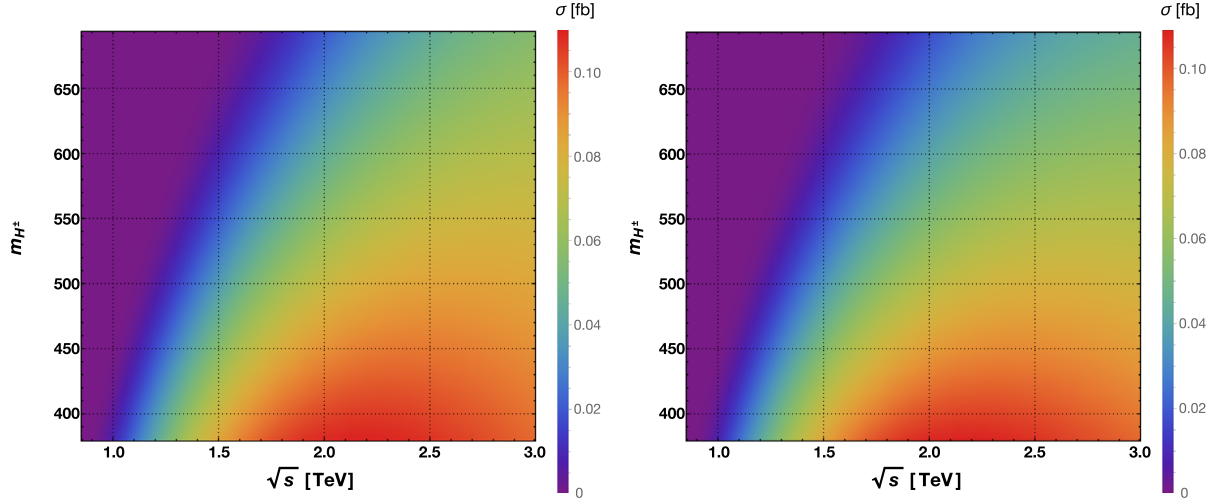
FIG. 3.   The cross section is given for the unpolarized incoming beams as a function of the $m_{H^\pm}$ and $\sqrt{s}$ in the non-alignment scenario. The scan is done for $t_\beta = 45$ and $m_{H^\pm}$ is calculated by varying the m_{H^0}. (left): $c_{\beta\alpha} = 0.1$ and Type-I couplings, (right): $c_{\beta\alpha} = 0.01(\frac{150}{m_{H^0}})^2$ and Type-II couplings are considered.

Since each of them were a function of t_β, they were boosted at high-t_β values in type I. Comparing the two plots in Fig. 3, the cross section in type I (left) and type II (right) got larger at low-$m_{H^\pm}$ values, and it declined at high $m_{H^\pm}$. On the other hand, the fall was a little bit faster in type II due to the $1/t_\beta$ dependence of the couplings.

The last analysis for this scenario is drawn in Fig. 4, in which the unpolarized cross section at $\sqrt{s} = 2.5$ TeV as a function of $m_{H^\pm}$ and t_β is given. If type-I Yukawa couplings are chosen, the distribution of the cross section in Fig. 4 (left) shows a small dependence on the t_β at high-t_β values compared to type II, Fig. 4 (right). On the (right), the cross section does not change much with t_β, but the change is dramatic with $m_{H^\pm}$. The situation in type I happens due to

the large values of the t_β in $c_{e\bar{e}[h^0,H^0]}$ and $c_{\nu_e\bar{e}H^+}$ couplings (through ζ_L) and $m_{H^\pm}$ dependence of the $c_{H^+H^-[h^0,H^0]}$ couplings. In each case, the cross section gets up to $\sigma_{UU} \approx 0.113$ fb at low-$m_{H^\pm}$ values. However, at smaller c.m. energies, the distinction between them completely disappears even at high-t_β values.

B. Low-m_H scenario

In this scenario, CP-even states are flipped, where the H^0 state is considered as the one that behaves like the SM Higgs boson. The computation is carried out for $t_\beta = 1.5$, and quartic parameters are taken as $Z_4 = Z_5 = -5$ so that the CP-even Higgs states are decoupled from A^0 and $H^\pm$. According to Eq. (76) in Ref. [63], that configuration also
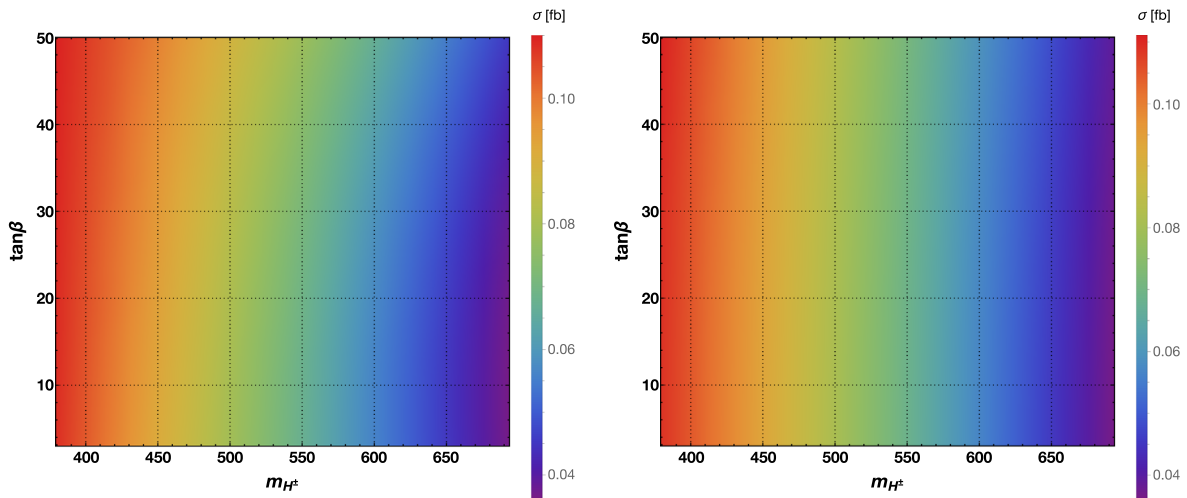

FIG. 4.   The unpolarized cross section at $\sqrt{s} = 2.5$ TeV as a function of the $m_{H^\pm}$ and t_β in the nonalignment scenario; (left): Type-I Yukawa couplings with $c_{\beta\alpha} = 0.1$, (right): Type-II Yukawa couplings with $c_{\beta\alpha} = 0.01(\frac{150}{m_H})^2$ are set.
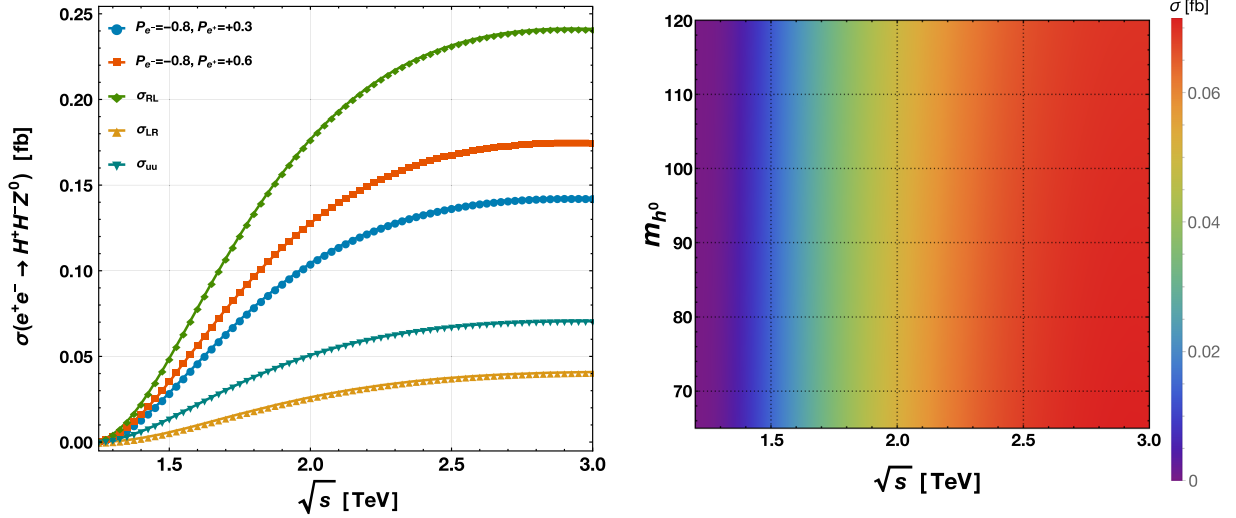
FIG. 5.   The cross section distributions in the low-m_H scenario, in which $m_{h^0} = 95$ GeV. (left): The process as a function of $\sqrt{s}$ is plotted for various polarizations depicted in the plot. (right): The cross section as a a function of light Higgs mass (m_{h^0}) and $\sqrt{s}$.

agrees with the vacuum stability and the perturbativity constraints. The cross section as a function of $\sqrt{s}$ is given in Fig. 5 (left). The unpolarized cross section gets up to 0.071 fb at $\sqrt{s} = 3.0$ TeV and then falls down, while the polarized cross sections are $\sigma_{LR} \approx 0.041$ fb and $\sigma_{RL} \approx 0.241$ fb. The same with the nonalignment scenario, the cross section is maximized for the configuration of right-handed polarized e^+ and left-handed polarized e^- beams. The unpolarized cross section as a function of the light Higgs mass (m_{h^0}) and $\sqrt{s}$ is plotted in Fig. 5 (right). It should be noted that, due to the small mass range for the light Higgs ($65 < m_{h^0} < 120$ GeV), the cross section changes very slowly with m_{h^0}, and the difference is around -6% at $\sqrt{s} = 2$ TeV between the lower and the higher m_{h^0} values. Besides these, the distribution of the cross section in type I and type II are the same in the numerical precision. When the exact alignment is chosen ($s_{\beta\alpha} = 1$), the t_β dependence of the cross section drops out over all in the calculation. The couplings $c_{e\bar{e}[h^0,H^0]}$ and $c_{\nu_e\bar{e}H^+}$ are a function of tb via ζ_L. Since the Yukawa scheme is relevant for the couplings between Higgses and fermions, these couplings do not affect the calculation even varying at this range. Moreover, even if we lose the exact alignment and set $s_{\beta\alpha} = 0.9$, the change in the cross section is around -2.5% at $\sqrt{s} = 1.5$ TeV, and it falls at high c.m. energies. Finally, we get $\sigma_{\text{pol-1}} \approx 0.143$ fb and $\sigma_{\text{pol-2}} \approx 0.175$ fb for the polarized incoming beams.

C. Region favored by recent experimental constraints

The last set of analyses is presented considering the results obtained from the recent experiments, particularly the flavor physics. In this scenario, there is no splitting between the charged Higgs mass, CP-odd Higgs mass, and the heavier CP-even Higgs masses ($m_H = m_{H^0} = m_{A^0} = m_{H^\pm}$). The

light CP-even state is assumed to be the SM one, the exact alignment limit is used ($s_{\beta\alpha} = 1$), and two parameters (t_β and $m_{H^\pm}$) given in Table V are regarded as a free parameters. The c.m. energy dependence of the cross section for unpolarized and polarized incoming beams is given in Fig. 6 up to $\sqrt{s} = 3$ TeV. On the left, the cross section for polarized beam configurations is plotted the same as in the previous figures, the type-I Yukawa coupling scheme is set, all the extra Higgs masses are set to $m_H = 175$ GeV, and $t_\beta = 10$ is taken. According to Ref. [24], the restrictions on the charged Higgs mass in type I are much looser compared to type II, and it is 150 GeV $< m_{H^\pm}$. Because of the possibility of having a smaller charged Higgs mass, the cross section gets much higher compared to the previous scenarios. The unpolarized cross section is calculated as $\sigma_{UU} \approx 0.278$ fb, and the cross section (σ_{RL}) particularly for $P_{e^+e^-} = (+1, -1)$ goes up to 0.978 fb. The polarized cross section is obtained as $\sigma_{\text{pol-1}} \approx 0.577$ fb and $\sigma_{\text{pol-2}} \approx 0.707$ fb.

The type-II Yukawa coupling structure is set in Fig. 6 (right), and due to the restrictions from the flavor observables, charged Higgs mass is constrained from below ($m_{H^\pm} > 500$ GeV). The production rate is lowered compared to type I, and the unpolarized cross section is $\sigma_{UU} = 0.073$ fb. However, the polarized cross section is obtained as $\sigma_{\text{pol-1}} \approx 0.151$ fb and $\sigma_{\text{pol-2}} \approx 0.185$ fb. In each case given in Fig. 6, polarization of the incoming beams enhances the cross section by a factor of 2.1 (2.5) for pol-1 (pol-2) compared to the unpolarized one.

The last result is given in Fig. 7, in which the cross section at $\sqrt{s} = 3.0$ TeV is plotted as a function of t_β and $m_{H^\pm}$. On the left side, the type-I Yukawa structure is set, and on the right, the type-II Yukawa structure is used. In type I, the cross section gets high for small charged Higgs masses, and it gets low as usual for high-$m_{H^\pm}$ values.
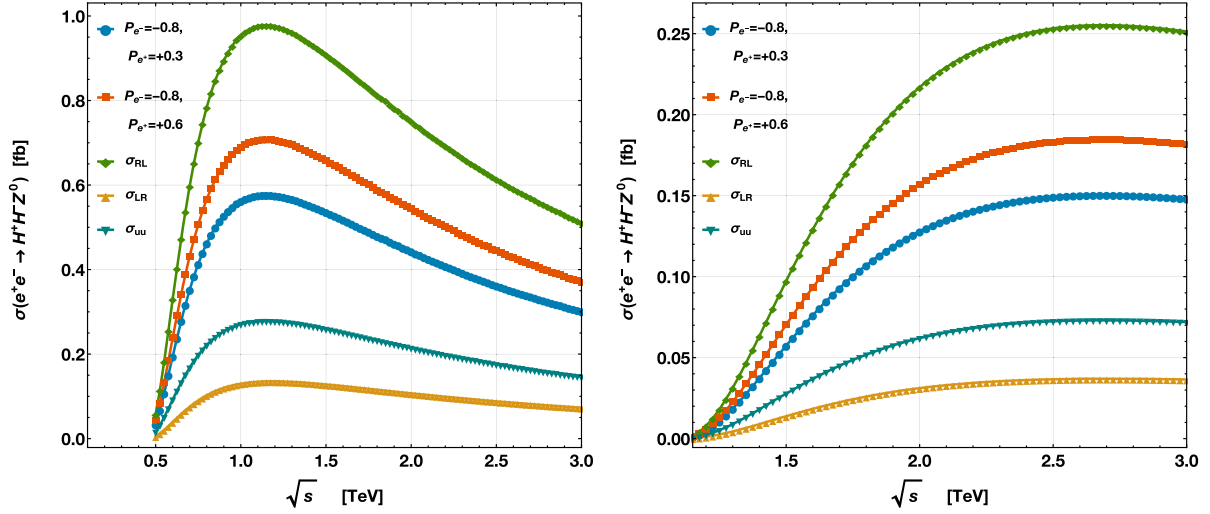
FIG. 6.   The cross section distributions are plotted in favor of the current experiments in the flavor physics. (left): The cross section of the process as a function of $\sqrt{s}$ for various polarized beam configurations is plotted, where the type-I Yukawa coupling scheme is set, $m_H = 175$ GeV and $t_\beta = 10$. (right): The same caption as the left figure, but type II and $m_H = 500$ GeV are set.
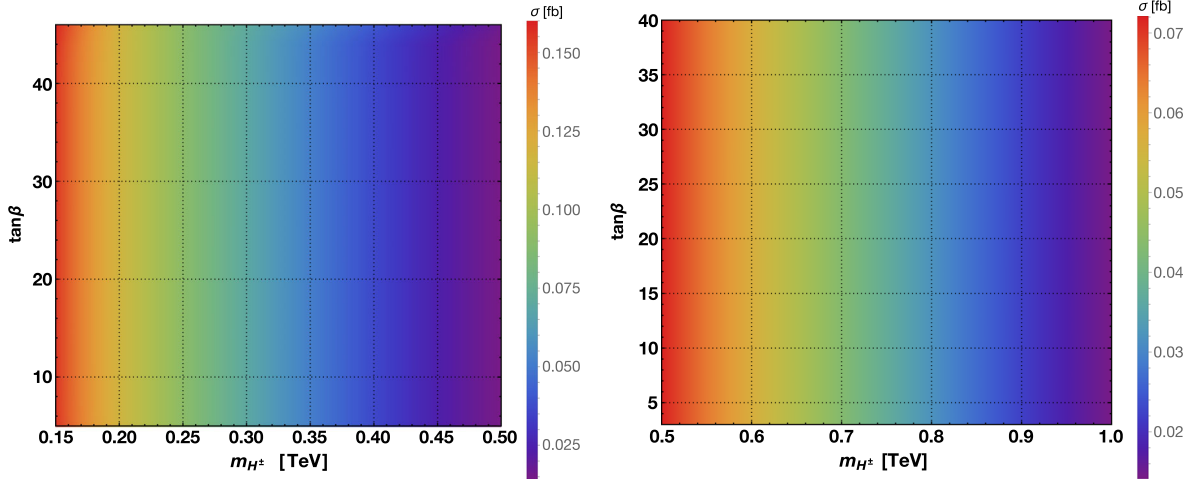

FIG. 7.   The cross section distributions for the last scenario called the favored region in the recent experimental constraints. The distributions are at $\sqrt{s} = 3$ TeV, $s_{\beta\alpha} = 1$, and all the extra Higgs masses are taken as $m_H = m_{H^0} = m_{A^0} = m_{H^\pm}$. (left): Type-I Yukawa couplings. (right): Type-II Yukawa couplings are set.

However, as can be seen clearly in both of the Fig. 7 plots, t_β does not affect the cross section. That means couplings given in Table I that have t_β dependence indirectly through s_β and c_β and directly in ζ_L do not influence the cross section in this special decoupling and exact alignment limit ($s_{\beta\alpha} = 1$). Comparing the two plots at $m_{H^\pm} = 500$ GeV shows that the cross section in type I is higher by 25%.

VI. IDENTIFYING THE PROCESS AT THE DETECTOR

In this section, the decay channels of the charged Higgs boson are discussed for all the three scenarios, and possible

collider signatures for measuring the process are examined. To explore the process in a collider, primarily, we need to detect all the possible charged Higgs products. The charged Higgs boson decays through $H^+ \to t\bar{b}$ in all three scenarios commonly with varying branching ratios. The other channels are $H^+ \to W^+ h^0$, $H^+ \to W^+ H^0$, and $H^+ \to \tau^+ \nu_\tau$. Besides that, various differential distributions of the charged Higgs and Z^0 boson are calculated, and discussion is carried out as to whether they could be used for selection in the detector. Finally, the possible background channels and challenges are indicated for the detection of the process in the collider. According to Ref. [64], Z^0 boson decays through three main channels with the following branching ratios: hadronic

(≈ 0.70), leptonic (≈ 0.10), and invisible (≈ 0.20). In addition to that, the W boson has hadronic ($\mathcal{B}(W \to \text{hadronic}) \approx 0.67$) and leptonic $\mathcal{B}(W \to l\nu_l) \approx 0.21$ decays (e and μ).

A. Decay channels of $H^\pm$ in the nonalignment scenario

In the nonalignment scenario, depending on the free parameters of the model, the charged Higgs boson decays mainly in the decay channels $H^+ \to t\bar{b}$ and $H^+ \to W^+ H^0$ in type I, and another channel is joined to them in type I, which is $H^+ \to W^+ h^0$. In Figs. 8 and 9, the branching ratios are drawn as a function of m_H and t_β with type I and II Yukawa coupling schemes. It can be seen that the decay of $H^+ \to W^+ h^0$ is going down while $H^+ \to W^+ H^0$ becomes dominant. A seesaw between the decays of $H^+ \to W^+ h^0$ and $H^+ \to W^+ H^0$ appears. $\mathcal{B}(H^+ \to W^+ H^0)$ is greater than 90% in the region $m_H \lesssim 350$ GeV and $t_\beta \gtrsim 6$. Then, it gradually decreases at high-m_H values, and the decay channel $H^+ \to W^+ h^0$ gains weight.

In the nonalignment scenario with type I, the process becomes $e^+ e^- \to H^+ H^- Z \to W^+ h^0 W^- h^0 Z$, and the hadronic decays of W and Z^0 bosons could be an ideal option for reconstructing the process at $m_H \gtrsim 500$ GeV given in Fig. 8. Since h^0 decays mostly through $\mathcal{B}(h^0 \to b\bar{b}) \approx 62\%$ and $\mathcal{B}(h^0 \to W^+ W^-) \approx 20\%$, and considering the $Z \to q\bar{q}$,

the final state of the process in this region will be four jets + four b-tagged jets + two jets (coming from Z^0 boson). The heavier CP-even Higgs boson with various decay channels is given in Fig. 8 (second row). The charged Higgs decays through the heavier CP-even Higgs boson and W boson for $m_H \lesssim 500$ GeV, and then H^0 most likely decays to vector boson pairs (WW/ZZ) or $h^0 h^0$ pairs. Considering the hadronic decays of the vector bosons and h^0, for the low m_H region, there will be in total 12 jets at the final state and also the decay products of the Z^0 boson (two jets or two leptons). Apparently, this scenario produces many jets at the final state, and it is a challenge to reconstruct the W boson, so the charged Higgses. The performance of the jet-finding algorithms in such a jetty environment is vital to studying the production and the couplings of the charged Higgs. Nonalignment with type I has the potential to produce the highest number of jets in the final state among all other cases presented in this study.

The situation is less complicated in type II; the charged Higgs decays through $H^+ \to t\bar{b}$ at high-m_H and -t_β values, and the decay channel $H^+ \to W^+ H^0$ gains weight at the low-m_H and -t_β region given in Fig. 9. Besides, $\mathcal{B}(H^0 \to b\bar{b}) \gtrsim 90\%$ in most of the parameter space. An ideal case for this scenario would be allowing H^0 decays through $b\bar{b}$ quarks and hadronic decay of the $W^\pm / Z^0$ bosons. Then,
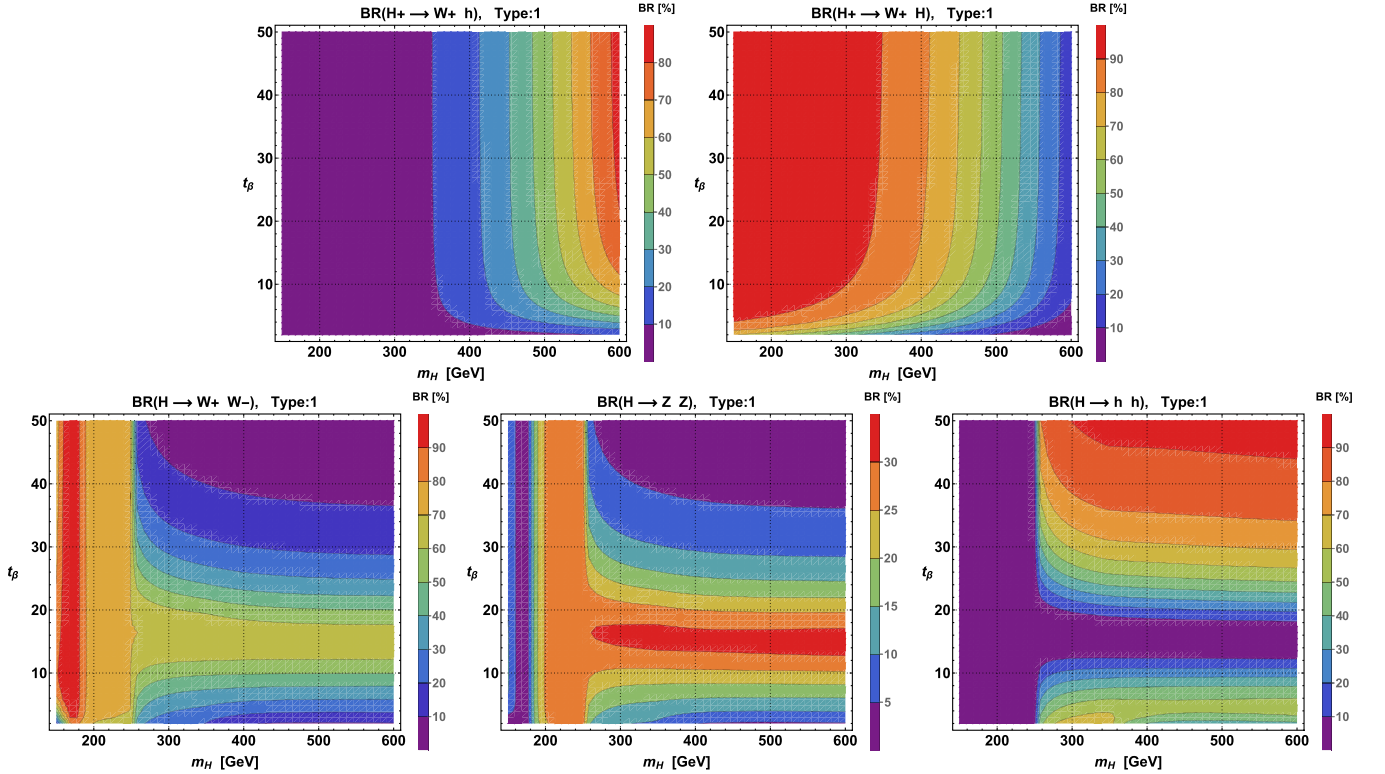

FIG. 8. Distributions are plotted for the branching ratios of the charged Higgs boson and CP-even H^0 boson in the nonalignment scenario. Decay channels are indicated in each figure. All the extra Higgs masses are taken as $m_H = m_{A^0} = m_{H^\pm}$, and m_{H^0} is calculated with the help of Eq. (12). Type-I Yukawa couplings are assumed, and $c_{\beta\alpha} = 0.1$ is set. (first row): Decays of $H^\pm$ are plotted. (second row): Decays of the CP-even H^0 boson are plotted.
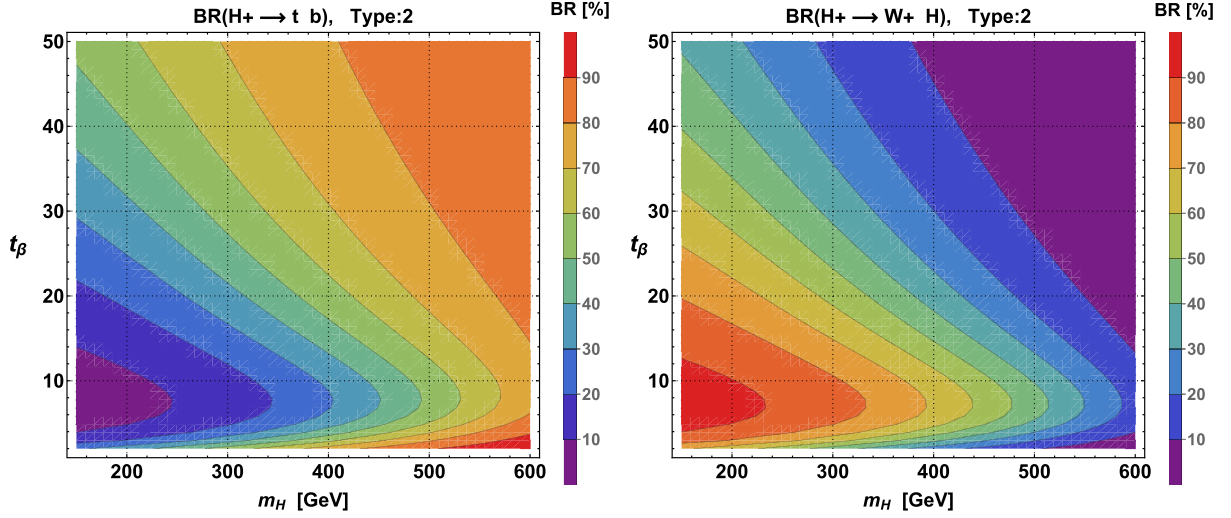
FIG. 9.   Distributions for the branching ratios of the charged Higgs boson in the nonalignment scenario. Decay channels are indicated in each figure. The Higgs masses are taken as $m_H = m_{A^0} = m_{H^\pm}$, and m_{H^0} is calculated with the help of Eq. (12). The calculation is carried out for $c_{\beta\alpha} = 0.01(\frac{150\text{ GeV}}{m_{H^0}})^2$, and type-II Yukawa couplings are assumed.

there will be four b-tagged jets + six jets in the final state. Additionally, it is possible to trigger the events with $Z \to l\bar{l}$, and there will be two leptons with opposite sign in the final state. Unfortunately, the branching ratio of the leptonic decays of the Z^0 boson is small compared to the hadronic decays. The decay channel $H^+ \to t\bar{b}$ is significant at high-m_H values. Then, the task is to look for top quarks in the final state. Consequently, the subsequent decays of $t \to Wb$, $W^\pm \to q\bar{q}(l\nu_l)$ will form the signature of the charged Higgs boson at a detector. If we let $Z \to q\bar{q}$ or $l\bar{l}$, the process $e^+e^- \to H^+H^-Z^0 \to tbtbZ$ could be reconstructed with ten jets + two b-tagged jets or eight jets + two b-tagged jets + two leptons, respectively. It is seen that tagging the b quark and reconstructing the charged Higgs mass with the possible decay products of the W boson is vital for the process. Another choice, which is common in the next scenarios as well, is to let W decay leptonically, and instead of two jets in the final states, there will be a lepton + missing E_T. However, a Monte Carlo simulation study would be the best to determine the efficiency of the leptonic decay channel.

B. Decay channels of $H^\pm$ in the low-m_H scenario

In the low-m_H scenario, the mass gap between the CP-even Higgs bosons is small, and the charged Higgs boson decays via two channels $H^+ \to W^+h^0$ and $H^+ \to t\bar{b}$ in both types I and II. The branching ratios for each type are given In Fig. 10, and the sum of $\mathcal{B}(H^+ \to W^+h^0)$ and $\mathcal{B}(H^+ \to t\bar{b})$ adds up to unity in this scenario. It is $\mathcal{B}(h^0 \to b\bar{b}) \gtrsim 80\%(90\%)$ in type I (type II). If $h^0 \to b\bar{b}$ is considered, the process could be tagged with four b-tagged jets + four jets + a Z^0 boson in both of the Yukawa coupling schemes (types I and II).

C. Decay channels of $H^\pm$ in the favored region

In this scenario, the charged Higgs boson decays via two channels $H^+ \to t\bar{b}$ and $H^+ \to \tau\nu_\tau$ for both types I and II. In Fig. 11, it can be seen that the $\mathcal{B}(H^+ \to t\bar{b})$ is the dominant decay channel for each Yukawa structure. Then, the same final state will be obtained with the nonalignment scenario type II. The subsequent decays of $t \to Wb$ and $W^\pm \to q\bar{q}(l\nu_l)$ form the final state of the charged Higgs boson. Then, considering the $Z \to q\bar{q}$, the final state of the process is four jets + four b-tagged jets + two jets.

D. Differential distributions

In this section, the differential cross sections are calculated as a function of the kinematical variables for each scenario, and a comparison is performed. The computation is carried out at $\sqrt{s} = 3$ TeV; $s_{\beta\alpha}$ or $c_{\beta\alpha}$ is taken from the corresponding table given for each scenario. Higgs masses are set to $m_{H^0} = 425$ GeV ($t_\beta = 45$) in the nonalignment scenario, $m_{h^0} = 80$ GeV in the low-m_H scenario, and $m_H = m_{H^0} = m_{A^0} = m_{H^\pm} = 175(500)$ GeV for type I (type II) in the favored region. $t_\beta = 10$ is set for all the scenarios. In Fig. 12 (left), the differential cross section as a function of the rapidity of the Z^0 boson is presented. It can be seen that the Z^0 boson is produced more likely in the central region compared to the high rapidities for all the scenarios. If a rapidity cut of $|y_Z| \le 2$ on the Z^0 boson is applied, then depending on the scenario, ≈75%–88% of the events could be captured. That shows it could be a useful kinematical cut to eliminate more events in the background. In Fig. 12 (center), distribution for the differential cross section as a function of the transverse momentum of the Z^0 boson (p_T^Z) is plotted for each scenario. According to the p_T^Z distribution, the Z^0 boson is produced more likely with
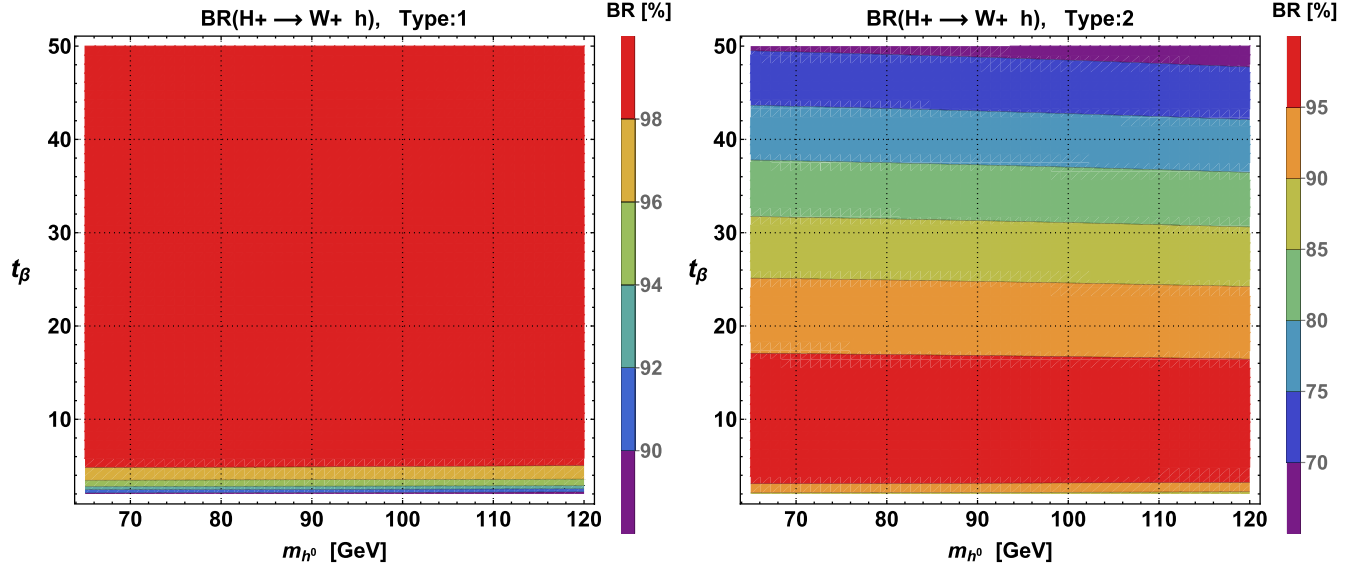
FIG. 10. Distributions for the branching ratios of the charged Higgs boson in the low-m_H scenario. Distributions are given for $c_{\beta\alpha} = 1$, $m_{H^0} = 125$ GeV, and accordingly $m_{A^0} = m_{H^\pm}$ are calculated with the help of Eq. (12). (left): Type-I Yukawa couplings are assumed. (right): Type-II Yukawa couplings are assumed.
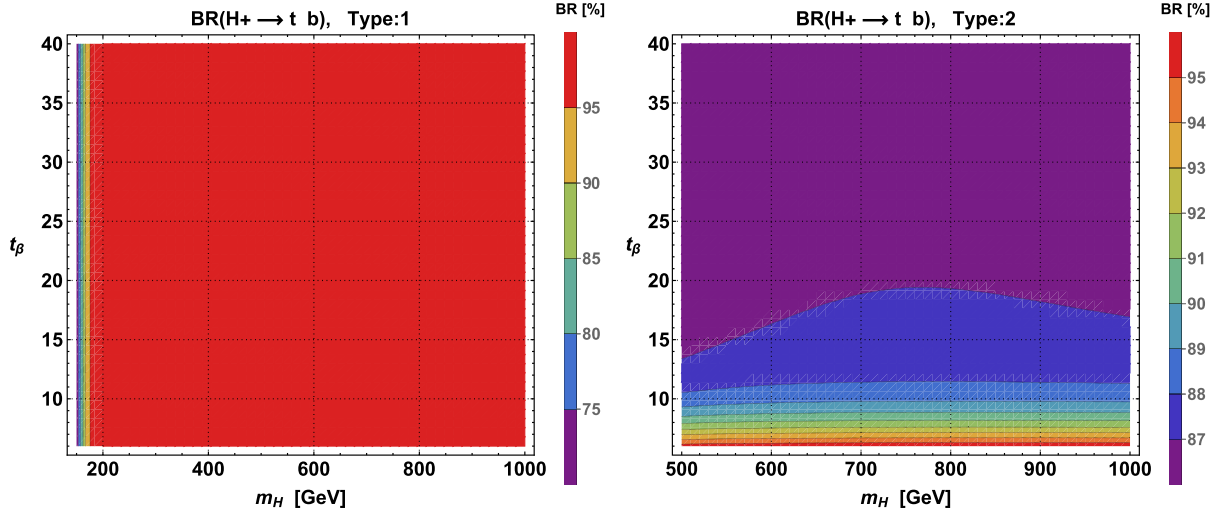

FIG. 11. Distributions for the branching ratios of the charged Higgs boson in the region favored by the recent experimental constraints. Distributions are for $s_{\beta\alpha} = 1$, and all the extra Higgs masses are taken as $m_H = m_{H^0} = m_{A^0} = m_{H^\pm}$. (left): Type-I Yukawa couplings are set. (right): Type-II Yukawa couplings are set.

small transverse momentum. That will most certainly affect the kinematical properties of the decay products of the Z^0 boson. Applying a cut of $p_T^Z < 400$ GeV reaps more than $\approx 70\%$ of the events. At last, the differential rate as a function of the rapidity difference of the charged Higgses is plotted in Fig. 12 (right), and it shows that the charged Higgses are produced very likely with a small rapidity difference, and $\approx 95\%$ of the events fall in $|\Delta y_{H^-H^+}| \leq 2$. Moreover, the normalized rate is the same in all the scenarios.

E. SM backgrounds

The production of $H^+H^-Z^0$ in the e^+e^- collider has a small cross section as it is presented in the previous section. Regarding the weakness of the signal, one may wonder if such a process could be extracted from the SM background. The decay chains of the charged Higgs in each scenario showed that the b-quark identification is vital in the reconstruction of the signal. Besides, the number of jets and the b-tagged jets at the final state in real world are not fixed due to the parton branching of the quarks and the
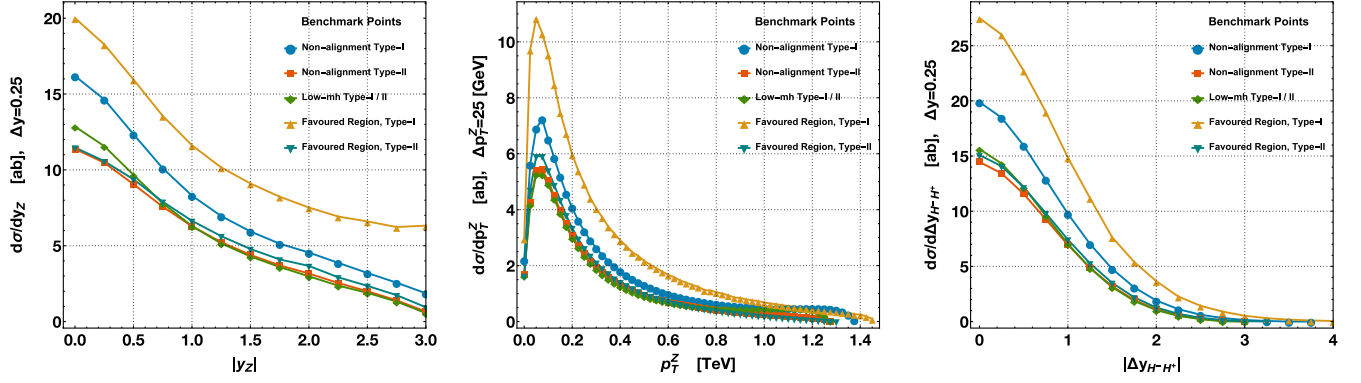
FIG. 12. The differential cross section as a function of the kinematical properties of Z and $H^{\pm}$ bosons where $\sqrt{s} = 3$ TeV, and the rest of the parameters are indicated in the text for each scenario. (left): $d\sigma/d|y_Z|$ distribution. (center): $d\sigma/dp_T^Z$ distribution. (right): $d\sigma/d|\Delta y_{H^-H^+}|$ distribution.

efficiency of the b tagging as well as the misidentification of them. By considering these points, there are many background channels that will shadow the process. Therefore, a large background is expected mainly from $e^+e^- \rightarrow q\bar{q}$, later these quarks will hadronize to jets. Moreover, $e^+e^- \rightarrow q\bar{q}Z$, $e^+e^- \rightarrow t\bar{t}$, and $e^+e^- \rightarrow t\bar{t}Z$ will contribute to the main background. On the other hand, the following processes could also contribute to the background. These are $e^+e^- \rightarrow t\bar{t}b\bar{b}b\bar{b}$ along with the Z^0 boson or multiple numbers of light jets (u, d, c, or s-type quark), $e^+e^- \rightarrow t\bar{t}ZH$, $e^+e^- \rightarrow t\bar{t}ZZ$, $e^+e^- \rightarrow t\bar{t}HH$, $e^+e^- \rightarrow t\bar{t}b\bar{b}Z$, and $e^+e^- \rightarrow W^+HW^-HZ$.

Hadronic decays of the $W^{\pm}/Z^0$ boson along with the jets could mimic the final state of the process. It looks like the top quark is essential for reconstructing the charged Higgs as well as in the elimination of the various background channels. Besides, it is also possible to allow the leptonic decays of $W^{\pm}/Z^0$ bosons. However, since the branching ratios are small, the multiplication of $\mathcal{B}(W \rightarrow l\nu_l)^2 \cdot \mathcal{B}(Z \rightarrow l\bar{l}) \approx 4.4 \times 10^{-3}$ reduces the cross section by $\sim 1/225$. Eventually, exploring the hadronic decays of $W^{\pm}/Z^0$ bosons gives more events in the detector. Therefore, jet-finding algorithms will determine whether the process could be measured due to the challenges in the high jet multiplicity. The full reconstruction of W, t, and $H^{\pm}$ and better efficiency of b-tagging certainly boost the discrimination power of extracting the signal from the background. The observability of the process $e^+e^- \rightarrow H^+H^-Z^0$ would require Monte Carlo simulation of the signal and all possible background processes, which is beyond the scope of this paper.

VII. CONCLUSIONS

In this paper, we have calculated the process $e^+e^- \rightarrow H^+H^-Z^0$ at the tree level in the 2HDM. The process is analyzed for three scenarios motivated by the current experimental constraints. They are the nonalignment

scenario, the low-m_H scenario, and the scenario inspired from the results in the flavor physics. In the nonalignment scenario, the unpolarized cross section has the value of 0.071 (0.106) fb depending on the Yukawa coupling scheme type II (type I). In the low-m_H scenario, the unpolarized cross section gets a value of 0.071 fb, and contrary to the other scenarios, the Yukawa coupling scheme does not have an impact. In the last scenario, which is motivated by the observables measured in the flavor physics, the unpolarized cross section gets a value of 0.279 (0.073) fb depending on the Yukawa coupling scheme type I (type II). Comparing each scenario shows that the cross section is enhanced to a factor of 2–2.5 depending on the scenario for the left-handed polarized electron beam ($P_{e^-} = -0.80$) and right-handed polarized positron beams ($P_{e^+} = +0.60$). The option of upgrading the incoming electron and the positron beam to be polarized has the power to enhance the potential of the machine. If it is assumed that CLIC could produce a total integrated luminosity of $\mathcal{L} \sim 3$ ab^{-1} at $\sqrt{s} = 3$ TeV [30], then there could be more than $\sim 2.7 \times 10^3$ events assuming polarization.

The decay channels of the charged Higgs boson in each scenario are also investigated with the help of 2HDMC. The analysis shows that some channels come forward such as $H^+ \rightarrow t\bar{b}$, $H^+ \rightarrow W^+h^0$, and $H^+ \rightarrow W^+H^0$. The subsequent hadronic decays of the top quark, $W^{\pm}/Z^0$ bosons, and h^0/H^0 bosons have a higher branching ratio compared to the leptonic ones. In that case, the final state of the process contains six jets + four b-tagged jets in the nonalignment scenario with type I and six jets + eight b-tagged jets in type II. Moreover, the other two scenarios have the same final state though following different decays, and there are six jets + four b-tagged jets in the end. Unfortunately, since the number of jets in the final state is high, it will be hard to reconstruct the process, and that is the most significant disadvantage. High efficiency in b tagging and reconstructing the $W^{\pm}/Z^0$ boson then reconstructing the top quark is vital for the charged Higgs

detection. Further, a charged Higgs pair has a higher production rate compared to the extra Z^0 boson in the final state. Considering the background, a detailed Monte Carlo study is required to determine the significance and the acceptance of the signal in a detector. Some differential distributions for the charged Higgs and Z^0 boson are presented, but the best selection cuts with a higher elimination of the background signals require a full detector simulation and maybe the help of the artificial neural networks.

The LHC experiment confirmed the existence of a neutral Higgs boson [38,40–42]; hereafter, the discovery of another scalar and even a charged one at the future colliders would be clear evidence of the existence of new physics beyond the SM. In recent years, the LHC experiment provided many results but no hint of the new physics yet. Since the precision measurements on Higgs and extended Higgs sector are a primary motivation for the LCC, this study shows the ability of the measurements for the process and particularly the charged Higgs sector of the 2HDM. Studying the production of $H^+H^-Z^0$ also revealed that the dominant contribution to the cross section in the low-m_{h^0} scenario and the scenario of the favored region are coming from the pair of the charged Higgs couplings to neutral CP-even Higgses. Thus, the process itself is useful to determine and confirm the couplings $c_{H^+H^-h^0}$ and $c_{H^+H^-H^0}$.

ACKNOWLEDGMENTS

[1] G. C. Branco, P. M. Ferreira, L. Lavoura, M. N. Rebelo, M. Sher, and J. P. Silva, Phys. Rep. **516**, 1 (2012).

[2] J. F. Gunion, H. E. Haber, G. L. Kane, and S. Dawson, Front. Phys. **80**, 1 (2000).

[3] S. Laurila (CMS Collaboration), Proc. Sci. CHARGED2016 (**2017**) 008.

[4] S. Kanemura, H. Yokoya, and Y.-J. Zheng, Nucl. Phys. **B886**, 524 (2014).

[5] A. Arhrib and G. Moultaka, Nucl. Phys. **B558**, 3 (1999).

[6] A. Arhrib, R. Benbrik, and C.-W. Chiang, Phys. Rev. D **77**, 115013 (2008).

[7] Y.-B. Liu and X.-L. Wang, Nucl. Phys. **B839**, 294 (2010).

[8] J. F. Shen and J. Cao, J. Phys. G **41**, 105003 (2014).

[9] H. E. Haber and D. O'Neil, Phys. Rev. D **74**, 015018 (2006); **74**, 059905(E) (2006).

[10] S. Davidson and H. E. Haber, Phys. Rev. D **72**, 035004 (2005); **72**, 099902(E) (2005).

[11] M. Carena and H. E. Haber, Prog. Part. Nucl. Phys. **50**, 63 (2003).

[12] L. J. Hall and M. B. Wise, Nucl. Phys. **B187**, 397 (1981).

[13] N. G. Deshpande and E. Ma, Phys. Rev. D **18**, 2574 (1978).

[14] L. Lavoura, Phys. Rev. D **50**, 7089 (1994).

[15] H. E. Haber, G. L. Kane, and T. Sterling, Nucl. Phys. **B161**, 493 (1979).

[16] E. Asakawa, D. Harada, S. Kanemura, Y. Okada, and K. Tsumura, Phys. Lett. B **672**, 354 (2009).

[17] J. F. Gunion and H. E. Haber, Phys. Rev. D **67**, 075019 (2003).

[18] M. Carena, I. Low, N. R. Shah, and C. E. M. Wagner, J. High Energy Phys. 04 (2014) 015.

[19] P. S. Bhupal Dev and A. Pilaftsis, J. High Energy Phys. 12 (2014) 024; 11 (2015) 147(E).

[20] J. Bernon, J. F. Gunion, H. E. Haber, Y. Jiang, and S. Kraml, Phys. Rev. D **92**, 075004 (2015).

[21] A. Alloul, N. D. Christensen, C. Degrande, C. Duhr, and B. Fuks, Comput. Phys. Commun. **185**, 2250 (2014).

[22] C. Degrande, Comput. Phys. Commun. **197**, 239 (2015).

[23] D. Eriksson, J. Rathsman, and O. Stal, Comput. Phys. Commun. **181**, 189 (2010).

[24] T. Enomoto and R. Watanabe, J. High Energy Phys. 05 (2016) 002.

[25] J. Kublbeck, H. Eck, and R. Mertig, Nucl. Phys. B, Proc. Suppl. **29**, 204 (1992); **29**, 204 (1992).

[26] T. Hahn, Comput. Phys. Commun. **140**, 418 (2001).

[27] T. Hahn and M. Rauch, Nucl. Phys. B, Proc. Suppl. **157**, 236 (2006); **157**, 236 (2006).

[28] J. Kublbeck, M. Bohm, and A. Denner, Comput. Phys. Commun. **60**, 165 (1990).

[29] K. Fujii et al., arXiv:1506.05992.

[30] M. J. Boland et al. (CLICdp and CLIC Collaborations), arXiv:1608.07537.

[31] I. Ginzburg and I. Ivanov, Phys. Rev. D **72**, 115010 (2005).

[32] A. W. El Kaffas, W. Khater, O. M. Ogreid, and P. Osland, Nucl. Phys. **B775**, 45 (2007).

[33] M. Sher, Phys. Rep. **179**, 273 (1989).

[34] N. G. Deshpande and E. Ma, Phys. Rev. D **18**, 2574 (1978).

[35] S. Nie and M. Sher, Phys. Lett. B **449**, 89 (1999).

[36] A. W. El Kaffas, W. Khater, O. M. Ogreid, and P. Osland, Nucl. Phys. **B775**, 45 (2007).

[37] S. Chatrchyan et al., Phys. Lett. B **716**, 30 (2012).

[38] G. Aad et al. (ATLAS Collaboration), Phys. Lett. B **716**, 1 (2012).

[39] V. Khachatryan et al. (CMS Collaboration), Eur. Phys. J. C **74**, 3076 (2014).

[40] S. Chatrchyan et al. (CMS Collaboration), Phys. Lett. B **716**, 30 (2012).

[41] V. Khachatryan et al. (CMS Collaboration), Eur. Phys. J. C **75**, 212 (2015).

[42] G. Aad *et al.* (ATLAS Collaboration), Eur. Phys. J. C **76**, 6 (2016).

[43] S. Schael *et al.* (SLD Electroweak Group, DELPHI, ALEPH, SLD, SLD Heavy Flavour Group, OPAL, LEP Electroweak Working Group, and L3 Collaborations), Phys. Rep. **427**, 257 (2006).

[44] M. E. Peskin and T. Takeuchi, Phys. Rev. Lett. **65**, 964 (1990).

[45] M. E. Peskin and T. Takeuchi, Phys. Rev. D **46**, 381 (1992).

[46] H. E. Haber and D. O'Neil, Phys. Rev. D **83**, 055017 (2011).

[47] J. F. Gunion and H. E. Haber, Phys. Rev. D **67**, 075019 (2003).

[48] W. Grimus, L. Lavoura, O. M. Ogreid, and P. Osland, Nucl. Phys. **B801**, 81 (2008).

[49] N. Polonsky and S. Su, Phys. Lett. B **508**, 103 (2001).

[50] G. Abbiendi *et al.* (LEP, DELPHI, OPAL, ALEPH, and L3 Collaborations), Eur. Phys. J. C **73**, 2463 (2013).

[51] G. Abbiendi *et al.* (LEP, DELPHI, OPAL, ALEPH, and L3 Collaborations), Eur. Phys. J. C **73**, 2463 (2013).

[52] V. M. Abazov *et al.* (D0 Collaboration), Phys. Rev. Lett. **102**, 191802 (2009).

[53] V. M. Abazov *et al.* (D0 Collaboration), Phys. Rev. D **80**, 071102 (2009).

[54] V. M. Abazov *et al.* (D0 Collaboration), Phys. Rev. D **80**, 051107 (2009).

[55] T. Aaltonen *et al.* (CDF Collaboration), Phys. Rev. Lett. **103**, 101803 (2009).

[56] G. Aad *et al.* (ATLAS Collaboration), J. High Energy Phys. 06 (2012) 039.

[57] S. Chatrchyan *et al.* (CMS Collaboration), J. High Energy Phys. 07 (2012) 143.

[58] S. Moretti, Proc. Sci., CHARGED2016 (**2016**) 014.

[59] A. W. El Kaffas, P. Osland, and O. M. Ogreid, Nonlin. Phenom. Complex Syst. (Dordrecht, Neth.) **10**, 347 (2007).

[60] A. W. El Kaffas, P. Osland, and O. M. Ogreid, Phys. Rev. D **76**, 095001 (2007).

[61] A. G. Akeroyd, Phys. Lett. B **368**, 89 (1996).

[62] V. D. Barger, J. L. Hewett, and R. J. N. Phillips, Phys. Rev. D **41**, 3421 (1990).

[63] H. E. Haber and O. Stål, Eur. Phys. J. C **75**, 491 (2015); **76**, 312(E) (2016).

[64] S. Eidelman *et al.* (Particle Data Group Collaboration), Phys. Lett. B **592**, 1 (2004).